
RAISING THE BAR ON THE EVALUATION OF OUT-OF-DISTRIBUTION DETECTION

A PREPRINT

Jishnu Mukhoti*
University of Oxford &
Meta AI

Tsung-Yu Lin
Meta AI

Bor-Chun Chen
Meta AI

Ashish Shah
Meta AI

Philip H.S. Torr
University of Oxford

Puneet K. Dokania [†]
University of Oxford

Ser-Nam Lim [†]
Meta AI

ABSTRACT

In image classification, a lot of development has happened in detecting out-of-distribution (OoD) data. However, most OoD detection methods are evaluated on a standard set of datasets, arbitrarily different from training data. There is no clear definition of what forms a “good” OoD dataset. Furthermore, the state-of-the-art OoD detection methods already achieve near perfect results on these standard benchmarks. In this paper, we define 2 categories of OoD data using the subtly different concepts of perceptual/visual and semantic similarity to in-distribution (iD) data. We define *Near OoD* samples as perceptually similar but semantically different from iD samples, and *Shifted* samples as points which are visually different but semantically akin to iD data. We then propose a GAN based framework for generating OoD samples from each of these 2 categories, given an iD dataset. Through extensive experiments on MNIST, CIFAR-10/100 and ImageNet, we show that **a**) state-of-the-art OoD detection methods which perform exceedingly well on conventional benchmarks are significantly less robust to our proposed benchmark. Moreover, **b**) models performing well on our setup also perform well on conventional real-world OoD detection benchmarks and vice versa, thereby indicating that one might not even need a separate OoD set, to reliably evaluate performance in OoD detection.

Keywords Out-of-Distribution Detection, Image Classification

1 Introduction

With the wide-spread deployment of deep learning models in real-life applications like autonomous driving Filos et al. [2020] and medical diagnosis Roy et al. [2021], it is imperative to ensure that in addition to being accurate, such models are also able to reliably quantify their uncertainty and identify inputs which they “don’t know”. One of the major applications of such uncertainty quantification methods is the detection of inputs sampled from a distribution different from the model’s training distribution (i.e, Out-of-Distribution or OoD inputs). A lot of work has been done in this direction from the perspective of uncertainty quantification Liu et al. [2020a], Van Amersfoort et al. [2020], Mukhoti et al. [2021], Lakshminarayanan et al. [2016], OoD Detection Hendrycks and Gimpel [2016], Lee et al. [2018], Fort et al. [2021], Winkens et al. [2020], Liang et al. [2017], Pinto et al. [2022], open-set recognition Liu et al. [2019], Mundt et al. [2019] and the like.

Since any point outside the training distribution can be considered OoD, the set of potential OoD inputs is infinite. This makes evaluating OoD detection a particularly challenging problem. The general evaluation practice involves using a proxy OoD dataset which is different from the training distribution (or in-distribution (iD) samples) to simulate an out-of-distribution scenario. The OoD detection algorithm is then evaluated on how well it can separate the iD samples from the OoD points. For the purposes of evaluation and benchmarking, it is then natural to ask which proxy OoD

*Preliminary work. Contact: jishnu.mukhoti@eng.ox.ac.uk

[†]Primary mentors, alphabetical order.

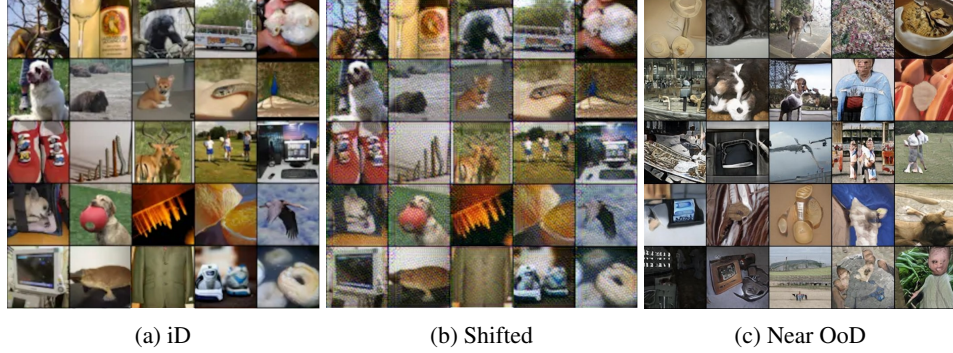


Figure 1: *Shifted* and *Near OoD* samples obtained from ImageNet. *Shifted samples* are visually different but semantically similar to the iD data. *Near OoD images* are perceptually similar to iD data but are semantically dissimilar.

dataset is best suited for measuring model performance. To answer this question, we need to consider the different types of OoD inputs that can arise in a real-world scenario.

In image classification, we model the conditional categorical distribution $p(y|\mathbf{x})$ over classes, given an input image \mathbf{x} . Under the i.i.d assumption, both the training and test images are assumed to be sampled from the same continuous distribution in image space, i.e., $p_{\text{train}}(\mathbf{x}) = p_{\text{test}}(\mathbf{x})$. In case of OoD samples, this assumption is broken, i.e., $p_{\text{train}}(\mathbf{x}) \neq p_{\text{oob}}(\mathbf{x})$. Based on the conditional distribution $p(y|\mathbf{x})$, we can then define two kinds of OoD samples.

Distribution Shift: Although the distribution in image space is different, the conditional distribution over class labels remains the same, i.e., $p_{\text{train}}(y|\mathbf{x}) = p_{\text{oob}}(y|\mathbf{x})$, and $p_{\text{train}}(\mathbf{x}) \neq p_{\text{oob}}(\mathbf{x})$. Such samples are generally derived from the training set by applying transformations like corruptions Hendrycks and Dietterich [2019] and semantic shifts Xiao et al. [2020], Koh et al. [2021], where the transformed images have the same labels as the originals from the training set. For example, ImageNet-C/P Hendrycks and Dietterich [2019] contain synthetic corruptions and perturbations applied to ImageNet Deng et al. [2009]. Such datasets provide a controlled environment to study models under specific synthetic and real-world distribution shifts.

Unseen Categories: The second category of OoD comprise images of classes which the model has not been trained on, i.e., $p_{\text{train}}(y|\mathbf{x}) \neq p_{\text{oob}}(y|\mathbf{x})$, and $p_{\text{train}}(\mathbf{x}) \neq p_{\text{oob}}(\mathbf{x})$. For a given training set, any dataset having a disjoint set of labels qualifies as OoD with unseen categories. How do we then decide which OoD dataset is good for evaluation? The convention is to use a well-known set of (iD vs OoD) dataset pairs like MNIST Lecun et al. [1998] vs Fashion-MNIST Xiao et al. [2017], CIFAR-10 Krizhevsky et al. [2009] vs SVHN Netzer et al. [2011] etc. However, **firstly**, the choice of these dataset pairs is relatively arbitrary and there is no guarantee that performance on these benchmarks will generalise to the real-world. **Secondly**, in recent literature Fort et al. [2021], Winkens et al. [2020], the terms “Near OoD” and “Far OoD” have been used to indicate the difficulty of an OoD detection task with Near OoD datasets (CIFAR-10 vs CIFAR-100) being more difficult than Far OoD (CIFAR-10 vs SVHN). With no model-agnostic metric quantifying the “nearness” of an OoD dataset, these terms are also not well-defined. **Finally**, the current state-of-the-art OoD detection baseline, Vision Transformer Fort et al. [2021], obtains around 96% AUROC on CIFAR-100 vs CIFAR-10 and over 99.5% AUROC on CIFAR-10 vs SVHN. Hence, the most popular OoD detection benchmarks are saturated and might give us the impression that state-of-the-art baselines are robust to OoD. The near perfect AUROC scores also indicate that these benchmarks might be rendered redundant in future for evaluating the performance of even better OoD detection methods which outperform the Vision Transformer Fort et al. [2021].

In this work, we thus aim to take a step towards improving the conventional evaluation process for OoD detection in image classification. We first look at the two types of OoD mentioned above through the lens of *perceptual/visual similarity* and *semantic similarity* Deselaers and Ferrari [2011], Brust and Denzler [2018] between images. Perceptual similarity between two images denotes how visually similar they are and semantic similarity captures the similarity of concepts that they represent. With this in mind, we define:

1. **Shifted sets** as perceptually dissimilar but semantically similar to the training distribution.
2. **Near OoD sets** as perceptually similar but semantically dissimilar to the training distribution.
3. **Far OoD sets** as both perceptually and semantically dissimilar to the training distribution.

Clearly, images which are both perceptually and semantically similar to the training distribution would be iD. We show the hierarchy of OoD samples in fig. 2. In this work, we particularly focus on generating Shifted and Near OoD sets. Given the training set, it is difficult to define a single distance measure in the image space which can capture both perceptual and semantic similarity. Hence, we propose using a sampling based generative model, a

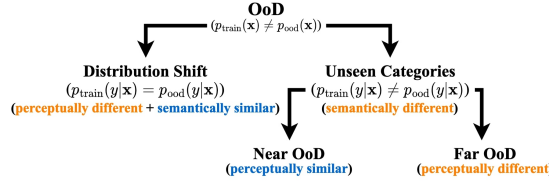


Figure 2: Categories of OoD samples

Generative Adversarial Network (GAN) Goodfellow et al. [2014] and design regularisers for the GAN objective using the definitions above to generate OoD samples.

For a training set $\mathcal{D} = (\mathbf{x}_i, y_i)_{i=1}^N$, where $y_i \in \mathcal{S}$, $\forall i$, in order to generate *shifted samples*, we learn a transformation $t_{\text{shift}} : \mathbf{x} \rightarrow \hat{\mathbf{x}}$ in the image space, $\mathbf{x}, \hat{\mathbf{x}} \in \mathbb{R}^{H, W, C}$, such that \mathbf{x} and $\hat{\mathbf{x}}$ are perceptually different and semantically similar, i.e., have the same label: $\text{argmax}_c p(y_c|\mathbf{x}) = \text{argmax}_c p(y_c|\hat{\mathbf{x}})$. This is an Image-to-Image translation problem and hence, we use a Pix2Pix Isola et al. [2017] model to learn a distribution shift. In case of *Near OoD*, we want to learn a distribution in the close perceptual vicinity of \mathcal{D} . This can be seen as a transformation $t_{\text{near ood}} : \mathbf{z} \rightarrow \hat{\mathbf{x}}$, $\mathbf{z} \sim \mathcal{N}(0, \mathbf{I})$ where the generated image $\hat{\mathbf{x}}$ is perceptually similar to the training distribution but does not belong to any of the iD classes: $\text{argmax}_c p(y_c|\hat{\mathbf{x}}) \notin \mathcal{S}$. This is an Image generation problem and hence, we use a GAN for generating Near OoD samples. In fig. 1, we show examples from ImageNet of shifted as well as Near OoD samples. Through extensive experiments using several OoD detection baselines comparing our benchmarks with conventional ones, we make the following observations and contributions.

Firstly, the performance of state-of-the-art OoD detection baselines (Deep Ensembles Lakshminarayanan et al. [2016] and Vision Transformers Fort et al. [2021]), established to be relatively robust on standard benchmarks, is consistently worse on our proposed benchmarks for both distribution shift and unseen category scenarios. This is true across datasets of all sizes: ImageNet, CIFAR-10/100 and MNIST, thereby showing that *there's still plenty of room for improvement in OoD detection research*. **Secondly**, we observe a consistent trend where models which perform better on our benchmarks also perform well on standard real-world benchmarks and vice versa. Assuming that standard benchmarks are indicative of real-world OoD detection performance, the fact that our benchmarks have been created without the use of any external OoD dataset then indicates that *one might not need an OoD dataset to measure OoD detection performance*. **Finally**, we propose a novel way to generate benchmarks for the evaluation of any OoD detection method.

2 Related Work

State-of-the-art on OoD Detection: As mentioned in Section 1, the task of uncertainty quantification naturally serves as a solution for OoD detection as OoD inputs should intuitively be assigned higher uncertainty. From this perspective, a lot of work has been done to model scalable deep neural networks to quantify their uncertainty. A popular thread of work in this regard uses the softmax distribution from a neural network to capture uncertainty. This starts off from Hendrycks and Gimpel [2016] where the authors simply use the softmax probability as uncertainty and continues on to several methods including augmentations Liang et al. [2017], Hsu et al. [2020], Lee et al. [2017], calibration Guo et al. [2017], Mukhoti et al. [2020], Joy et al. [2022] and energy based models Liu et al. [2020b]. The advantage of these methods lies in the fact that they can quantify uncertainty using a single deterministic forward pass. However, the softmax distribution often fails to capture epistemic uncertainty Kendall and Gal [2017] and is overconfident on incorrect predictions for OoD inputs Gal [2016]. A more principled approach of quantifying uncertainty uses the Bayesian formalism Neal [2012] and is applied to deep neural nets using approximate Bayesian inference methods Gal and Ghahramani [2016], Blundell et al. [2015], Mandt et al. [2017]. Yet another popular uncertainty quantification method is deep ensembles Lakshminarayanan et al. [2016] which uses an ensemble of neural networks and averages the softmax distributions to compute uncertainty. Deep ensembles and its modifications Wen et al. [2020] have been widely accepted as one of the the state-of-the-art methods for uncertainty quantification. However, both approximate Bayesian inference and deep ensembles require either multiple forward passes at test time or multiple models to make predictions, thereby adding significant computational overhead. Attempting to achieve ensemble level performance from a single deterministic model, DUQ Van Amersfoort et al. [2020] and SNGP Liu et al. [2020a, 2022] develop distance-aware deterministic models which can quantify uncertainty. These methods perform competitively with deep ensembles without the additional computational overhead. More recently, RegMixup Pinto et al. [2022] showed that simply using the widely known mixup loss Zhang et al. [2018a] as a regularizer not only provides state-of-the-art OoD performance but also significantly improves the accuracy of a model. Finally, Fort et al. [2021] show that pre-trained Vision Transformers, when fine-tuned on a downstream dataset, achieve state-of-the-art AUROC scores on various conventional OoD benchmarks.

Conventional OoD evaluation: OoD samples are generally one of two types: i) *distribution shifted* samples and ii) samples which belong to an *unseen category* which the model hasn't been trained on. For evaluation, the general practice is to use separate OoD datasets for testing. For shifted samples, some of the well-known datasets include ImageNet-C (corrupted) and ImageNet-P (perturbed) Hendrycks and Dietterich [2019] which use synthetic corruptions and perturbations as well as stylised versions of ImageNet like ImageNet-R Hendrycks et al. [2020], ImageNet-Sketch Wang et al. [2019] etc. There are also datasets containing specific real-world shifts like WILDS Koh et al. [2021], Backgrounds Xiao et al. [2020], colored MNIST Gulrajani and Lopez-Paz [2020] etc. As shifted datasets retain the label information of the original dataset, models are evaluated on their calibration error Ovadia et al. [2019], which compares the model confidence with its accuracy on the provided test set. On the other hand, to test a model's performance on unseen categories, a separate OoD dataset is normally used. In the current literature, MNIST Lecun et al. [1998] vs Fashion-MNIST Xiao et al. [2017], CIFAR-10/100 vs SVHN & CIFAR-100/10 and ImageNet Deng et al. [2009] vs ImageNet-O Hendrycks et al. [2021] are the standard benchmarks for unseen distributions. Recently, Hendrycks et al. [2019] released the Species dataset as an OoD dataset for ImageNet-21K. However, the choice of these datasets is relatively arbitrary and a lot of the current OoD benchmarks including CIFAR-10 vs SVHN/CIFAR-100 and MNIST vs Fashion-MNIST are saturated Fort et al. [2021]. In this work, we thus show that generating OoD samples given a training set can produce significantly more challenging benchmarks for even the state-of-the-art OoD detection methods.

GAN for OoD: GANs have been previously used to generate samples on the boundary of image classes Lee et al. [2017], Dionelis [2021], Zaheer et al. [2020] as well as train the discriminator for anomaly detection Wang et al. [2018], Ngo et al. [2019]. The purpose is to either use the GAN itself for anomaly detection or use generated samples during training to improve the performance for OoD detection Kong and Ramanan [2021], Chen et al. [2021]. As mentioned before, with the lack of a clear definition of distance in image space, it is difficult to encode different types of OoD in a GAN and this is where one of our primary contributions lies. Secondly, our motivation is also orthogonal to these works. We use a GAN to improve the evaluation of OoD detection methods rather than improve the methods themselves.

3 Method

In this section, we formalise our approach to generate shifted and near OoD samples given a training set. First, we encode perceptual and semantic similarity as quantifiable loss functions for generative models. Then we discuss the GAN architectures and objective functions to generate shifted and Near OoD samples respectively.

Perceptual similarity as a loss function As mentioned in section 1, perceptual similarity between images represents how visually similar they are. Since we have target images from the training set, we can use a Full-Reference Image Quality Assessment (FR-IQA) Bosse et al. [2018] metric to encode perceptual loss. There exist several FR-IQA metrics in the literature like SSIM Wang et al. [2004], FSIM Zhang et al. [2011] and LPIPS Zhang et al. [2018b] but we use the *Learned Perceptual Image Patch Similarity* (LPIPS) Zhang et al. [2018b] as it is known to correlate with human judgement well. Let f_θ represent a pre-trained convolutional network. Given two images, \mathbf{x}_1 and \mathbf{x}_2 , the LPIPS computes the cosine distance between feature space activations of \mathbf{x}_1 and \mathbf{x}_2 across different layers of the network f_θ as shown below:

$$\mathcal{L}_{\text{LPIPS}}(\mathbf{x}_1, \mathbf{x}_2) = \sum_l \left(\frac{1}{H_l W_l} \|f_\theta^l(\mathbf{x}_1) - f_\theta^l(\mathbf{x}_2)\|_2^2 \right) \quad (1)$$

where $f_\theta^l(\mathbf{x}_1)$ and $f_\theta^l(\mathbf{x}_2) \in \mathbb{R}^{H_l, W_l, C_l}$ are the feature space representations from inputs \mathbf{x}_1 and \mathbf{x}_2 in layer l of the network. In this work, we use LPIPS with a VGG, although other architectures can be used as well. From here on out, we represent perceptual loss as $\mathcal{L}_{\text{LPIPS}}$. Minimizing $\mathcal{L}_{\text{LPIPS}}(\mathbf{x}_1, \mathbf{x}_2)$ encourages images \mathbf{x}_1 and \mathbf{x}_2 to be perceptually similar and vice versa.

Semantic similarity as a loss function In image classification, the semantic meaning of an image is encoded in its class label. To identify if an image is semantically similar to the training distribution, we need a model which understands the semantic meaning of the training distribution. However, a single classifier can make incorrect and confident predictions on inputs Guo et al. [2017], especially when they are not from any of the training classes Ovadia et al. [2019]. In this work, we take inspiration from Bayesian literature Neal [2012] and quantify semantic similarity, using the *mutual information* (MI) $\mathbb{I}[y, \theta | \mathcal{D}, \mathbf{x}]$, (also known as *information gain*) Gal [2016] between the posterior distribution over parameters of a Bayesian model $p(\theta | \mathcal{D})$ and its predicted distribution over classes $p(y | \mathbf{x}, \theta)$. Let (\mathbf{x}_g, y_g) be an input and \mathcal{S} be the set of training classes. If $y_g \in \mathcal{S}$, seeing the sample (\mathbf{x}_g, y_g) won't cause much information gain about the posterior $p(\theta | \mathcal{D})$. On the other hand, $y_g \notin \mathcal{S}$ will cause a high information gain about the posterior and $\mathbb{I}[y, \theta | \mathcal{D}, \mathbf{x}]$ will be high. Thus, in order to generate semantically similar/dissimilar images, we want $\mathbb{I}[y, \theta | \mathcal{D}, \mathbf{x}]$ to be low/high.

Due to the computational intractability of Bayesian inference in deep learning, we use a pre-trained deep ensemble which can be seen as a way to perform Bayesian Model Averaging Wilson and Izmailov [2020] with each model in the ensemble being a sample from the posterior. Following Gal [2016], we approximate MI as the difference

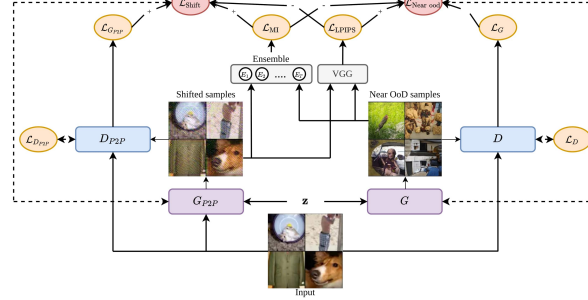


Figure 3: Schematic of the proposed method to generate Shifted and Near OoD samples. G_{P2P} and D_{P2P} represent the Pix-2-Pix to generate shifted samples and G and D represent the GAN to generate Near OoD images. The dotted lines show paths for gradient propagation.

between the entropy of the average softmax distribution of the ensemble and the average entropy of the softmax distributions of each individual network in the ensemble. Let $p(y|\mathbf{x}, \theta_t)$ represent the softmax distribution produced by the t^{th} network in an ensemble of T networks, on an input \mathbf{x} . The average softmax distribution for the ensemble is $p(y|\mathbf{x}, \theta) = \frac{1}{T} \sum_{t=1}^T p(y|\mathbf{x}, \theta_t)$. Then, the MI for the ensemble on input \mathbf{x} can be approximated as:

$$\mathcal{L}_{MI}(\mathbf{x}) = \hat{\mathbb{H}}[y, \theta | \mathcal{D}, \mathbf{x}] \approx \mathbb{H}[p(y|\mathbf{x}, \theta)] - \frac{1}{T} \sum_{t=1}^T \mathbb{H}[p(y|\mathbf{x}, \theta_t)] \quad (2)$$

where $\mathbb{H}[\cdot]$ represents the entropy of a distribution. We use \mathcal{L}_{MI} of a pre-trained ensemble as the semantic loss to quantify semantic similarity of an image to the training distribution. Semantically similar images (eg., images belonging to training classes) should have low \mathcal{L}_{MI} ³ and vice versa.

Generative Model Having defined perceptual and semantic similarity as quantifiable loss functions, we discuss two different GAN architectures for the two different types of OoD data. For distribution shift, we intend to learn a transformation on iD data and hence, use a conditional GAN architecture, Pix-2-Pix Isola et al. [2017] in particular. For Near OoD, we intend to learn a distribution instead and hence, use a standard GAN. We do not change the loss for the discriminator in any of the GANs and only regularise the loss for the generator to produce the desired OoD type.

Distribution Shift: For distribution shift, we want to maximize the perceptual loss \mathcal{L}_{LPIPS} (to generate perceptually different images) and minimize the semantic loss \mathcal{L}_{MI} (to preserve the semantic meaning of generated images). Thus, the regularised objective for the Pix-2-Pix generator is:

$$\begin{aligned} \mathcal{L}_{Shift} = & \underbrace{\mathbb{E}_{\mathbf{x}, \mathbf{z}} [\log(1 - D_{P2P}(\mathbf{x}, G_{P2P}(\mathbf{x}, \mathbf{z})))]}_{\text{Pix-2-Pix Generator Loss}} \\ & - \underbrace{\lambda_p \mathbb{E}_{\mathbf{x}, \mathbf{z}} [\mathcal{L}_{LPIPS}(\mathbf{x}, G_{P2P}(\mathbf{x}, \mathbf{z}))]}_{\text{maximize perceptual loss}} \\ & + \underbrace{\lambda_s \mathbb{E}_{\mathbf{x}, \mathbf{z}} [\mathcal{L}_{MI}(G_{P2P}(\mathbf{x}, \mathbf{z}))]}_{\text{minimize semantic loss}}, \end{aligned} \quad (3)$$

where G_{P2P} and D_{P2P} represent the generator and discriminator of the Pix-2-Pix GAN and λ_p and λ_s are the regularisation coefficients for the perceptual and semantic losses.

Near OoD: Similarly, for Near OoD, we want to minimize the perceptual loss \mathcal{L}_{LPIPS} (to encourage perceptually similar images) and maximize the semantic loss \mathcal{L}_{MI} (to generate semantically different images which don't belong to

³Interestingly, an alternative explanation of \mathcal{L}_{MI} can be found in uncertainty quantification literature Gal [2016]. MI is well-known to capture *epistemic uncertainty*, the type of uncertainty which occurs due to lack of data and reduces on observing more data. Hence, MI is high for OoD inputs with previously unseen categories. It is also used in active learning (the BALD metric) Gal et al. [2017], Kirsch et al. [2019] as an acquisition function to obtain informative samples from the pool set. Here, we maximise MI of a pre-trained ensemble as an objective function to generate OoD samples from unseen categories. i.e., semantically dissimilar samples with high epistemic uncertainty.

training set classes). We use a GAN for Near OoD distributions with the generator objective as shown below:

$$\begin{aligned}
 \mathcal{L}_{\text{Near ood}} = & \underbrace{\mathbb{E}_{\mathbf{z}}[\log(1 - D(G(\mathbf{z})))]}_{\text{GAN Generator Loss}} \\
 & + \underbrace{\lambda_p \mathbb{E}_{\mathbf{x}, \mathbf{z}}[\mathcal{L}_{\text{LPIPS}}(\mathbf{x}, G(\mathbf{z}))]}_{\text{minimize perceptual loss}} \\
 & - \underbrace{\lambda_s \mathbb{E}_{\mathbf{z}}[\mathcal{L}_{\text{MI}}(G(\mathbf{z}))]}_{\text{maximize semantic loss}}
 \end{aligned} \tag{4}$$

where G and D denote the generator and discriminator of the GAN respectively. See fig. 3 for a schematic.

4 Experiments

4.1 Implementation Details

Setting λ_p and λ_s and MI thresholding: In eq. (3) and eq. (4), we introduce the regularisation coefficients λ_p and λ_s . To set these, we generate samples using different combinations of λ_s and λ_p . We then measure the MI on the training ensemble for all generated samples and filter them such that MI is neither too high (avoid samples which are too dissimilar), nor too low (samples which coincide with iD). The lower bound is selected to be the lowest value which minimizes MI overlap between val and near OoD sets and the upper bound is chosen to be lower bound + 0.4 (see fig. 9 in appendix). In particular, we use [0.1, 0.5] for MNIST, [0.2, 0.6] for CIFAR-10 and [0.4, 0.8] for CIFAR-100 and ImageNet. We found these settings to empirically produce good OoD samples across datasets.

Ensemble for \mathcal{L}_{MI} : We implement the semantic loss \mathcal{L}_{MI} on MNIST using an ensemble of 4 different networks: LeNet Lecun et al. [1998], AlexNet Krizhevsky et al. [2012], VGG-11 Simonyan and Zisserman [2014] and ResNet-18 He et al. [2016]. On CIFAR-10/100, we use 6 networks: DenseNet-121 Huang et al. [2017], ResNet-50/110, VGG-16, Wide-ResNet-28-10 and Inception-v3 Szegedy et al. [2016] and on ImageNet, we use 3 networks: ResNet-18, MobileNet-v3-Large Howard et al. [2019] and EfficientNet-B0 Tan and Le [2019]. All the ensemble models are trained on their respective training sets.

Generating Near OoD Datasets We use a GAN to generate Near OoD samples from the training set using the $\mathcal{L}_{\text{Near ood}}$ loss. In particular, for MNIST, we use DCGAN for its simplicity and on CIFAR-10/100 and ImageNet, we use BigGAN due to its superior performance in terms of FID scores. For all the GANs, we set λ_p to 1 and perform a grid search for λ_s over the interval [0.5, 3] at steps of 0.25. As mentioned above, we use all the resulting trained GANs and filter samples out by thresholding on MI for the ensemble.

Generating Shifted Datasets We generate shifted samples using a Pix-2-Pix model trained on $\mathcal{L}_{\text{shift}}$ loss. After a grid search over different values, we found $\lambda_s = 1$ and $\lambda_p = 2$ to produce the best results on CIFAR-10 and ImageNet. Further training details can be found in appendix A. We show qualitative examples of both near OoD and shifted samples in fig. 1 and additional samples in appendix C.

4.2 Sanity Check on Benchmarks

We perform a sanity check using the CIFAR-10 dataset to verify that the Near OoD samples are indeed semantically dissimilar and perceptually similar while the Shifted samples are semantically similar and perceptually dissimilar.

Semantic similarity to the training distribution To verify that Near OoD samples are semantically dissimilar and Shifted samples are semantically similar to iD, we compare the predictions of an ensemble of 6 models: DenseNet-121, ResNet-50/110, VGG-16, Wide-ResNet-28-10 and Inception-v3 on the CIFAR-10 test set with both near OoD and shifted versions of CIFAR-10. Note that the ensembles are different from the ones used in training. We present the corresponding confusion matrices in fig. 4. Clearly, in case of shifted samples, the label information is preserved as the ensemble’s predicted classes broadly match the correct labels. However, such is not the case for near OoD samples where the predictions for each class are mostly incorrect indicating that the dataset has not preserved the label information from the training distribution.

Perceptual similarity to the training distribution To measure perceptual similarity between images, we use the well-known FID score Heusel et al. [2017]. We show the FID between the CIFAR-10 training set and Shifted (S) CIFAR-10 comparing with all the corruption types at intensity 5 of CIFAR-10-C Hendrycks and Dietterich [2019]. Similarly, we compare the FID of Near OoD (N) CIFAR-10 with SVHN, CIFAR-100 and samples generated by a BigGAN trained on CIFAR-10. We present the results in fig. 5. It is evident that S CIFAR-10 has a very high FID

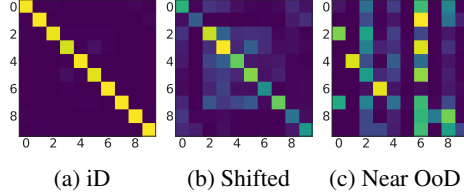


Figure 4: Confusion matrices for ensemble predictions on versions of CIFAR-10.

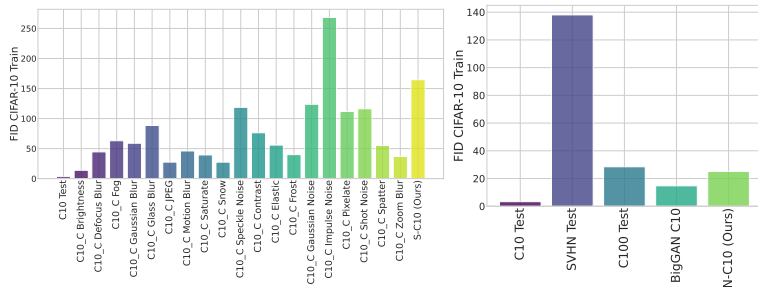


Figure 5: FID scores with CIFAR-10 training set on various OoD sets comparing with CIFAR-10 test set for reference.

Model	Im-O (SE)	Im-O (SC)	N-Im (Ours) (SE)	N-Im (Ours) (SC)
ViT-B-16	89.15	88.13	80.63	79.72
ViT-B-32	84.94	82.96	76.98	75.43
ViT-L-16	91.36	90.69	84.70	82.68
ViT-L-32	90.51	88.91	81.65	80.06

Table 1: AUROC % of ViT on ImageNet vs ImageNet-O (Im-O) and Near OoD ImageNet (N-Im) with softmax entropy (SE) and confidence (SC).

score indicating perceptual dissimilarity from the training set. Note however, that it is not the highest among all the corruption types in CIFAR-10-C. On the other hand, N CIFAR-10 has a significantly lower FID than SVHN and slightly lower than CIFAR-100, providing evidence in favour of the fact that N CIFAR-10 is perceptually more similar to the training set as compared to CIFAR-100 or SVHN.

4.3 Evaluating Near OoD Datasets

Next, we evaluate the Near OoD samples using two experiments. Firstly, we use state-of-the-art OoD detection methods Lakshminarayanan et al. [2016], Fort et al. [2021] on generated Near OoD datasets obtained from MNIST, CIFAR-10/100 and ImageNet and compare them with conventionally used OoD benchmarks. Secondly, we compare performance on models trained using outlier exposure Hendrycks et al. [2018] on our datasets with conventional ones.

OoD Detection Baselines For evaluation, we use state-of-the-art OoD detection methods. First, we use softmax entropy and softmax confidence Hendrycks and Gimpel [2016] as well as the Mahalanobis distance Lee et al. [2018] for models trained on the respective training sets. Second, we use 5-member deep ensembles, with predictive entropy Lakshminarayanan et al. [2016] as the measure of uncertainty. The predictive entropy of a deep ensemble is the entropy of the average softmax distribution (first term in eq. (2)). Note that the ensemble used to compute \mathcal{L}_{MI} during training contains models with different architectures to encourage variability in predictions. During evaluation however, the models in each ensemble have the same architecture. Finally, we use Vision Transformers Fort et al. [2021] with softmax confidence, entropy and Mahalanobis as the strongest baseline. On ImageNet, we only provide results using Vision Transformers.

Competitive Benchmarks For comparison, we use current conventional benchmarks. In particular, we compare with MNIST vs Fashion-MNIST, CIFAR-10 vs SVHN/CIFAR-100, CIFAR-100 vs SVHN/CIFAR-10 and ImageNet vs ImageNet-O Hendrycks et al. [2021]. We present the test set accuracies and AUROC scores for MNIST in table 4 of the appendix, CIFAR-10/100 and ImageNet test accuracies in table 5 of the appendix, corresponding AUROC scores for CIFAR-10/100 shown as bar plots in fig. 6 and finally, AUROC scores for ImageNet models in table 1. All related AUPRC scores are shown appendix B.

Observations Our observations are as follows:

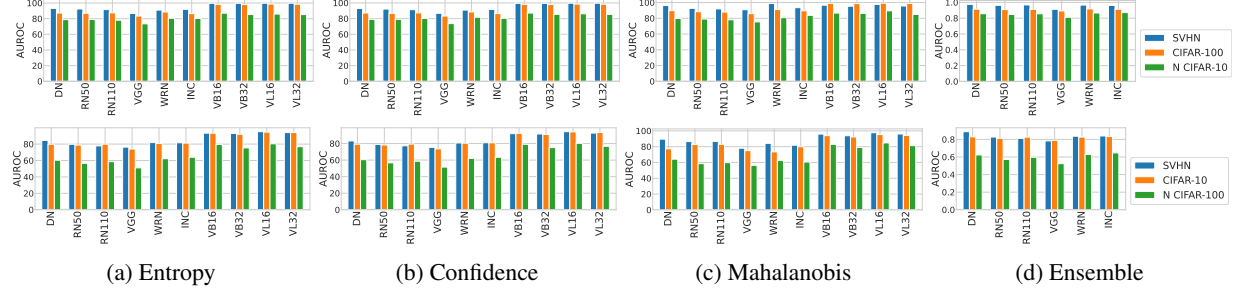


Figure 6: AUROC % for different models, DenseNet-121 (DN), ResNet-50 (RN50), ResNet-110 (RN110), VGG-16, Wide-ResNet-28-10 (WRN) and Inception-v3 (INC), ViT-B-16/32 (VB16/32) and ViT-L-16/32 (VL16/32) trained on CIFAR-10 (first row) and CIFAR-100 (second row) using SVHN, CIFAR-10/100 and Near OoD (N) CIFAR-10/100 as OoD datasets.

Model	Outlier Dataset	Test Accuracy	AUROC				AUPRC			
			SVHN		C10	N C100	Tiny-ImageNet		SVHN	C10
			SVHN	C10	N C100	Tiny-ImageNet	SVHN	C10	N C100	Tiny-ImageNet
ResNet-50	None	79.52	80.97	78.98	56.38	79.52	88.97	74.92	65.97	76.57
	SVHN	78.79	—	79.95	60.45	80.02	—	78.82	69.31	77.82
	C10	78.98	82.97	—	62.60	83.11	90.54	—	70.75	78.73
	N C100	78.82	87.02	81.65	—	84.40	94.51	82.81	—	80.70
Wide-ResNet-28-10	None	80.46	81.46	80.54	62.69	81.84	90.52	76.42	68.91	78.49
	SVHN	80.13	—	82.97	64.44	82.77	—	77.32	69.95	79.68
	C10	79.7	84.45	—	64.52	82.98	91.96	—	73.55	80.61
	N C100	79.92	87.23	84.31	—	85.63	92.88	79.22	—	81.42

Table 2: AUROC and AUPRC scores obtained by performing outlier exposure Hendrycks et al. [2018] on models trained on CIFAR-100 (C100). Models tuned using Near OoD CIFAR-100 (N C100) consistently obtain the highest AUROC and AUPRC scores.

Model	Im-val	Im-A	Im-v2	Im-C		Im-R	Im-Sketch	S Im (Ours)
				Avg ECE %	Max ECE %			
ViT-B-16	3.62	14.16	7.43	11.18	18.61	5.38	15.44	26.15
ViT-B-32	3.70	23.13	8.15	11.32	19.21	7.69	17.64	29.15
ViT-L-16	2.35	12.67	7.30	9.42	13.44	4.79	14.97	22.76
ViT-L-32	2.51	13.20	7.62	11.03	15.76	4.85	15.12	23.54

Table 3: ECE % on standard ImageNet (Im) shifts compared to our Shifted ImageNet (S Im).

1. *AUROC & AUPRC for all model architectures across all training datasets and all baselines are significantly lower for our Near OoD samples as compared to conventionally used OoD datasets.* This brings into question, the performance of baselines which are considered to be robust to OoD inputs, as evidenced from their performance on standard benchmarks. It also provides evidence in favour of more challenging OoD detection benchmarks for evaluation which are far from saturation.
2. *The order of performance is preserved.* If a model M_1 outperforms a model M_2 on our Near OoD benchmark, it broadly outperforms M_2 on all conventionally used real-world benchmarks and vice-versa.

Discussion & Visualisation Firstly, as mentioned before, conventional OoD benchmarks might become redundant in future for the best OoD detection methods. Our Near OoD datasets are much more effective at measuring performance as all the baselines consistently underperform on our samples. Secondly, even though the Near OoD samples might not look like real-world objects, the fact that the ordering of performance is preserved between our benchmarks and conventional ones implies that they can be used to estimate real-world OoD detection performance. We visualise Near OoD samples from 10 ImageNet classes in fig. 8 and observe that Near OoD images contain patches from original classes in an odd order which makes the images unrecognizable, while still preserving close perceptual proximity to original classes. We find this to be true in general for other classes too. In fact, we find that it is not necessary for an OoD image to represent a real-world object as long as it captures certain desirable properties. For near OoD, the desirable property is to be semantically dissimilar while lying in the close perceptual vicinity of the training distribution.

4.4 Outlier Exposure on Near OoD Datasets

In Hendrycks et al. [2018], exposure to outliers during training was proposed as a way to improve model performance on OoD datasets. In outlier exposure, models are trained on two datasets: i) the training set on which the loss is the usual cross-entropy loss and ii) the outlier dataset on which the loss is the cross-entropy between the softmax distribution and a uniform distribution over class labels. The assumption is that exposure to good outlier datasets will make the

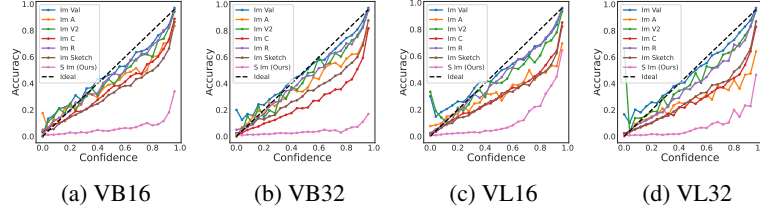


Figure 7: Reliability plots for ImageNet shifts



Figure 8: ImageNet Near OoD with class names

model detect any unseen outlier datasets as well. In this experiment, we want to see how models can improve on OoD detection performance once exposed to our generated near OoD samples as outliers.

To do this, we train a ResNet-50 and a Wide-ResNet-28-10 on CIFAR-100 using SVHN, CIFAR-10 and Near OoD CIFAR-100 as outlier datasets. Training details can be found in appendix A. For both models, we also compare with a baseline with no exposure to outliers. Finally, we use Tiny-ImageNet as an independent OoD dataset which is not used for outlier exposure. We present the test accuracy, AUROC and AUPRC scores for all models in table 2. *Again, we observe a clear ordering in performance improvement where models trained using Near OoD CIFAR-100 as outliers outperform models trained with CIFAR-100 as outliers, which in turn outperform models trained using SVHN as outliers. All models outperform the ones trained without any outliers.*

The above observation provides additional evidence to support the use of Near OoD samples, not just to benchmark OoD detection baselines, but also to improve them through outlier exposure. Furthermore, it corroborates our previous observation that even an image which does not represent any real world object can be very useful if it captures desirable properties in terms of semantic and perceptual similarity.

4.5 Evaluating Shifted Datasets

In this experiment, we evaluate our method of learning distribution shifts by comparing the shifted datasets with other well-known synthetic and real-world shifts. For CIFAR-10, we compare with CIFAR-10-C Hendrycks and Dietterich [2019] and for ImageNet, we compare with synthetic shifts: ImageNet-C, ImageNet-R (renditions) Hendrycks et al. [2020], ImageNet-Sketch Wang et al. [2019] and real-world shifts: ImageNet-A Hendrycks et al. [2021] and ImageNet-V2 Recht et al. [2019]. For CIFAR-10-C and ImageNet-C, we use corrupted images at the highest intensity 5.

We report the Expected Calibration Error (ECE) in table 11 of the appendix for CIFAR-10 models and table 3 for ImageNet. Detailed results for each corruption type can be found in appendix B. For each model, the ECE for every competitive dataset is starkly lower than the ECE obtained on our Shifted datasets. To better understand the effect of learned shifts, we compute the VGG LPIPS between the ImageNet val set and corruptions taken from ImageNet-C and from our method. Note that this is different from the FID analysis in fig. 5 as unlike FID, here, we are computing difference between individual pairs of images. We ensure that the L2 norm of the difference between normal and corrupted images is same (set to 50) for all corruption types. Results are in fig. 10a in the appendix. The high LPIPS for our shift suggests that the corruptions learnt are transformations which decreases perceptual similarity from the perspective of a neural net. At the same time, minimizing an ensemble’s MI in $\mathcal{L}_{\text{Shift}}$ encourages corruptions which make classifiers confident on their predictions. Hence, we have high ECE scores indicating miscalibrated models. This is further corroborated from the reliability plots for Shifted-ImageNet vs all other shifts in fig. 7, where for Shifted-ImageNet, models consistently have lower accuracy as compared confidence, i.e., they are overconfident and miscalibrated.

4.6 Evaluation of OoD detection in real life

Having evaluated our benchmarks, in order to use them in real-life applications, we need to verify if we can compare baselines sensibly using our benchmarks. Indeed that is the very purpose of a benchmark. We make the observation here that in all our experiments across datasets, the ordering of performance between baselines is broadly consistent between our benchmarks and the conventional ones. *Models which perform well on our benchmarks also perform well on conventional benchmarks and vice versa.* We show this particularly for ImageNet in a radar plot (fig. 10b in the appendix). Assuming that conventional OoD detection benchmarks generalise to and are indicative of real-world performance, we can then use the above observation as validation for the proposed benchmarks. Interestingly, this also shows that we might not need an OoD dataset in the first place to evaluate a model’s OoD detection performance. We could reliably estimate the OoD detection performance of any model just from the training set by following our proposed method.

5 Conclusion

Reliably evaluating the behaviour of models in unknown scenarios is an open problem and is extremely difficult because of infinitely many situations that could potentially fulfill our notion of “unknown” with respect to in-distribution. To our knowledge, our work is the very first step in the direction where we do not advocate the naive approach of testing on arbitrarily chosen “other” datasets. Rather we propose to learn the distribution of samples satisfying constraints mimicking our notion of what is out-of-distribution. Through numerous experiments, we show that our generated samples provide for a more challenging and reliable benchmark for even the current state-of-the-art OoD detection baselines.

6 Acknowledgements

Jishnu started this project as part of his internship at Meta AI (June 2021 - Sept 2021) and then continued working on it after returning to Oxford University. He was also employed part-time by Meta (Nov 2021 - Jan 2022) to work on this project. This work is also supported by the UKRI grant: Turing AI Fellowship EP/W002981/1 and EPSRC/MURI grant: EP/N019474/1. We would like to thank the Royal Academy of Engineering, FiveAI and Meta AI.

References

Angelos Filos, Panagiotis Tsigkas, Rowan McAllister, Nicholas Rhinehart, Sergey Levine, and Yarin Gal. Can autonomous vehicles identify, recover from, and adapt to distribution shifts? In *International Conference on Machine Learning*, pages 3145–3153. PMLR, 2020.

Abhijit Guha Roy, Jie Ren, Shekoofeh Azizi, Aaron Loh, Vivek Natarajan, Basil Mustafa, Nick Pawlowski, Jan Freyberg, Yuan Liu, Zach Beaver, et al. Does your dermatology classifier know what it doesn’t know? detecting the long-tail of unseen conditions. *arXiv preprint arXiv:2104.03829*, 2021.

Jeremiah Zhe Liu, Zi Lin, Shreyas Padhy, Dustin Tran, Tania Bedrax-Weiss, and Balaji Lakshminarayanan. Simple and principled uncertainty estimation with deterministic deep learning via distance awareness. *arXiv preprint arXiv:2006.10108*, 2020a.

Joost Van Amersfoort, Lewis Smith, Yee Whye Teh, and Yarin Gal. Uncertainty estimation using a single deep deterministic neural network. In *International Conference on Machine Learning*, pages 9690–9700. PMLR, 2020.

Jishnu Mukhoti, Andreas Kirsch, Joost van Amersfoort, Philip HS Torr, and Yarin Gal. Deterministic neural networks with appropriate inductive biases capture epistemic and aleatoric uncertainty. *arXiv preprint arXiv:2102.11582*, 2021.

Balaji Lakshminarayanan, Alexander Pritzel, and Charles Blundell. Simple and scalable predictive uncertainty estimation using deep ensembles. *arXiv preprint arXiv:1612.01474*, 2016.

Dan Hendrycks and Kevin Gimpel. A baseline for detecting misclassified and out-of-distribution examples in neural networks. *arXiv preprint arXiv:1610.02136*, 2016.

Kimin Lee, Kibok Lee, Honglak Lee, and Jinwoo Shin. A simple unified framework for detecting out-of-distribution samples and adversarial attacks. *Advances in neural information processing systems*, 31, 2018.

Stanislav Fort, Jie Ren, and Balaji Lakshminarayanan. Exploring the limits of out-of-distribution detection, 2021.

Jim Winkens, Rudy Bunel, Abhijit Guha Roy, Robert Stanforth, Vivek Natarajan, Joseph R Ledsam, Patricia MacWilliams, Pushmeet Kohli, Alan Karthikesalingam, Simon Kohl, et al. Contrastive training for improved out-of-distribution detection. *arXiv preprint arXiv:2007.05566*, 2020.

Shiyu Liang, Yixuan Li, and Rayadurgam Srikant. Enhancing the reliability of out-of-distribution image detection in neural networks. *arXiv preprint arXiv:1706.02690*, 2017.

Francesco Pinto, H Yang, Ser-Nam Lim, Philip HS Torr, and Puneet K Dokania. RegMixup: Mixup as a regularizer can surprisingly improve accuracy and out distribution robustness. In *NeurIPS*, 2022.

Ziwei Liu, Zhongqi Miao, Xiaohang Zhan, Jiayun Wang, Boqing Gong, and Stella X Yu. Large-scale long-tailed recognition in an open world. In *Proceedings of the IEEE/CVF Conference on Computer Vision and Pattern Recognition*, pages 2537–2546, 2019.

Martin Mundt, Sagnik Majumder, Iuliia Pliushch, Yong Won Hong, and Visvanathan Ramesh. Unified probabilistic deep continual learning through generative replay and open set recognition. *arXiv preprint arXiv:1905.12019*, 2019.

Dan Hendrycks and Thomas Dietterich. Benchmarking neural network robustness to common corruptions and perturbations. *arXiv preprint arXiv:1903.12261*, 2019.

Kai Xiao, Logan Engstrom, Andrew Ilyas, and Aleksander Madry. Noise or signal: The role of image backgrounds in object recognition. *arXiv preprint arXiv:2006.09994*, 2020.

Pang Wei Koh, Shiori Sagawa, Sang Michael Xie, Marvin Zhang, Akshay Balsubramani, Weihua Hu, Michihiro Yasunaga, Richard Lanas Phillips, Irena Gao, Tony Lee, et al. Wilds: A benchmark of in-the-wild distribution shifts. In *International Conference on Machine Learning*, pages 5637–5664. PMLR, 2021.

Jia Deng, Wei Dong, Richard Socher, Li-Jia Li, Kai Li, and Li Fei-Fei. Imagenet: A large-scale hierarchical image database. In *2009 IEEE conference on computer vision and pattern recognition*, pages 248–255. Ieee, 2009.

Y. Lecun, L. Bottou, Y. Bengio, and P. Haffner. Gradient-based learning applied to document recognition. *Proceedings of the IEEE*, 86(11):2278–2324, 1998. doi:10.1109/5.726791.

Han Xiao, Kashif Rasul, and Roland Vollgraf. Fashion-mnist: a novel image dataset for benchmarking machine learning algorithms. *arXiv preprint arXiv:1708.07747*, 2017.

Alex Krizhevsky, Geoffrey Hinton, et al. Learning multiple layers of features from tiny images. 2009.

Yuval Netzer, Tao Wang, Adam Coates, Alessandro Bissacco, Bo Wu, and Andrew Y Ng. Reading digits in natural images with unsupervised feature learning. 2011.

Thomas Deselaers and Vittorio Ferrari. Visual and semantic similarity in imagenet. In *CVPR 2011*, pages 1777–1784. IEEE, 2011.

Clemens-Alexander Brust and Joachim Denzler. Not just a matter of semantics: the relationship between visual similarity and semantic similarity. *arXiv preprint arXiv:1811.07120*, 2018.

Ian Goodfellow, Jean Pouget-Abadie, Mehdi Mirza, Bing Xu, David Warde-Farley, Sherjil Ozair, Aaron Courville, and Yoshua Bengio. Generative adversarial nets. *Advances in neural information processing systems*, 27, 2014.

Phillip Isola, Jun-Yan Zhu, Tinghui Zhou, and Alexei A Efros. Image-to-image translation with conditional adversarial networks. In *Proceedings of the IEEE conference on computer vision and pattern recognition*, pages 1125–1134, 2017.

Yen-Chang Hsu, Yilin Shen, Hongxia Jin, and Zsolt Kira. Generalized odin: Detecting out-of-distribution image without learning from out-of-distribution data. In *Proceedings of the IEEE/CVF Conference on Computer Vision and Pattern Recognition*, pages 10951–10960, 2020.

Kimin Lee, Honglak Lee, Kibok Lee, and Jinwoo Shin. Training confidence-calibrated classifiers for detecting out-of-distribution samples. *arXiv preprint arXiv:1711.09325*, 2017.

Chuan Guo, Geoff Pleiss, Yu Sun, and Kilian Q Weinberger. On calibration of modern neural networks. In *International Conference on Machine Learning*, pages 1321–1330. PMLR, 2017.

Jishnu Mukhoti, Viveka Kulharia, Amartya Sanyal, Stuart Golodetz, Philip HS Torr, and Puneet K Dokania. Calibrating deep neural networks using focal loss. *arXiv preprint arXiv:2002.09437*, 2020.

Tom Joy, Francesco Pinto, Ser-Nam Lim, Philip HS Torr, and Puneet K Dokania. Sample-dependent adaptive temperature scaling for improved calibration. In *ICML 2022 Workshop on Distribution-Free Uncertainty Quantification (DFUQ)*, 2022.

Weitang Liu, Xiaoyun Wang, John D Owens, and Yixuan Li. Energy-based out-of-distribution detection. *arXiv preprint arXiv:2010.03759*, 2020b.

Alex Kendall and Yarin Gal. What uncertainties do we need in bayesian deep learning for computer vision? *arXiv preprint arXiv:1703.04977*, 2017.

Yarin Gal. *Uncertainty in Deep Learning*. PhD thesis, University of Cambridge, 2016.

Radford M Neal. *Bayesian learning for neural networks*, volume 118. Springer Science & Business Media, 2012.

Yarin Gal and Zoubin Ghahramani. Dropout as a bayesian approximation: Representing model uncertainty in deep learning. In *international conference on machine learning*, pages 1050–1059. PMLR, 2016.

Charles Blundell, Julien Cornebise, Koray Kavukcuoglu, and Daan Wierstra. Weight uncertainty in neural network. In *International Conference on Machine Learning*, pages 1613–1622. PMLR, 2015.

Stephan Mandt, Matthew D Hoffman, and David M Blei. Stochastic gradient descent as approximate bayesian inference. *arXiv preprint arXiv:1704.04289*, 2017.

Yeming Wen, Dustin Tran, and Jimmy Ba. Batchensemble: an alternative approach to efficient ensemble and lifelong learning. *arXiv preprint arXiv:2002.06715*, 2020.

Jeremiah Zhe Liu, Shreyas Padhy, Jie Ren, Zi Lin, Yeming Wen, Ghassen Jerfel, Zack Nado, Jasper Snoek, Dustin Tran, and Balaji Lakshminarayanan. A simple approach to improve single-model deep uncertainty via distance-awareness. *arXiv preprint arXiv:2205.00403*, 2022.

Hongyi Zhang, Moustapha Cisse, Yann N. Dauphin, and David Lopez-Paz. mixup: Beyond empirical risk minimization. In *International Conference on Learning Representations*, 2018a. URL <https://openreview.net/forum?id=r1Ddp1-Rb>.

Dan Hendrycks, Steven Basart, Norman Mu, Saurav Kadavath, Frank Wang, Evan Dorundo, Rahul Desai, Tyler Zhu, Samyak Parajuli, Mike Guo, et al. The many faces of robustness: A critical analysis of out-of-distribution generalization. *arXiv preprint arXiv:2006.16241*, 2020.

Haohan Wang, Songwei Ge, Zachary Lipton, and Eric P Xing. Learning robust global representations by penalizing local predictive power. *Advances in Neural Information Processing Systems*, 32, 2019.

Ishaan Gulrajani and David Lopez-Paz. In search of lost domain generalization. *arXiv preprint arXiv:2007.01434*, 2020.

Yaniv Ovadia, Emily Fertig, Jie Ren, Zachary Nado, David Sculley, Sebastian Nowozin, Joshua V Dillon, Balaji Lakshminarayanan, and Jasper Snoek. Can you trust your model’s uncertainty? evaluating predictive uncertainty under dataset shift. *arXiv preprint arXiv:1906.02530*, 2019.

Dan Hendrycks, Kevin Zhao, Steven Basart, Jacob Steinhardt, and Dawn Song. Natural adversarial examples. In *Proceedings of the IEEE/CVF Conference on Computer Vision and Pattern Recognition*, pages 15262–15271, 2021.

Dan Hendrycks, Steven Basart, Mantas Mazeika, Mohammadreza Mostajabi, Jacob Steinhardt, and Dawn Song. Scaling out-of-distribution detection for real-world settings. *arXiv preprint arXiv:1911.11132*, 2019.

Nikolaos Dionelis. Omasgan: Out-of-distribution minimum anomaly score gan for sample generation on the boundary. *arXiv preprint arXiv:2110.15273*, 2021.

Muhammad Zaigham Zaheer, Jin-ha Lee, Marcella Astrid, and Seung-Ik Lee. Old is gold: Redefining the adversarially learned one-class classifier training paradigm. In *Proceedings of the IEEE/CVF Conference on Computer Vision and Pattern Recognition*, pages 14183–14193, 2020.

Chu Wang, Yan-Ming Zhang, and Cheng-Lin Liu. Anomaly detection via minimum likelihood generative adversarial networks. In *2018 24th International Conference on Pattern Recognition (ICPR)*, pages 1121–1126. IEEE, 2018.

Phuc Cuong Ngo, Amadeus Aristo Winarto, Connie Khor Li Kou, Sojeong Park, Farhan Akram, and Hwee Kuan Lee. Fence gan: Towards better anomaly detection. In *2019 IEEE 31st International Conference on Tools with Artificial Intelligence (ICTAI)*, pages 141–148. IEEE, 2019.

Shu Kong and Deva Ramanan. Opengan: Open-set recognition via open data generation. In *Proceedings of the IEEE/CVF International Conference on Computer Vision*, pages 813–822, 2021.

Guangyao Chen, Peixi Peng, Xiangqian Wang, and Yonghong Tian. Adversarial reciprocal points learning for open set recognition. *arXiv preprint arXiv:2103.00953*, 2021.

Sebastian Bosse, Dominique Maniry, Klaus-Robert Müller, Thomas Wiegand, and Wojciech Samek. Deep neural networks for no-reference and full-reference image quality assessment. *IEEE Transactions on Image Processing*, 27(1):206–219, 2018. doi:10.1109/TIP.2017.2760518.

Zhou Wang, Alan C Bovik, Hamid R Sheikh, and Eero P Simoncelli. Image quality assessment: from error visibility to structural similarity. *IEEE transactions on image processing*, 13(4):600–612, 2004.

Lin Zhang, Lei Zhang, Xuanqin Mou, and David Zhang. Fsim: A feature similarity index for image quality assessment. *IEEE transactions on Image Processing*, 20(8):2378–2386, 2011.

Richard Zhang, Phillip Isola, Alexei A Efros, Eli Shechtman, and Oliver Wang. The unreasonable effectiveness of deep features as a perceptual metric. In *Proceedings of the IEEE conference on computer vision and pattern recognition*, pages 586–595, 2018b.

Andrew G Wilson and Pavel Izmailov. Bayesian deep learning and a probabilistic perspective of generalization. *Advances in neural information processing systems*, 33:4697–4708, 2020.

Yarin Gal, Riashat Islam, and Zoubin Ghahramani. Deep bayesian active learning with image data. In *International Conference on Machine Learning*, pages 1183–1192. PMLR, 2017.

Andreas Kirsch, Joost Van Amersfoort, and Yarin Gal. Batchbald: Efficient and diverse batch acquisition for deep bayesian active learning. *Advances in neural information processing systems*, 32, 2019.

Alex Krizhevsky, Ilya Sutskever, and Geoffrey E Hinton. Imagenet classification with deep convolutional neural networks. *Advances in neural information processing systems*, 25:1097–1105, 2012.

Karen Simonyan and Andrew Zisserman. Very deep convolutional networks for large-scale image recognition. *arXiv preprint arXiv:1409.1556*, 2014.

Kaiming He, Xiangyu Zhang, Shaoqing Ren, and Jian Sun. Deep residual learning for image recognition. In *Proceedings of the IEEE conference on computer vision and pattern recognition*, pages 770–778, 2016.

Gao Huang, Zhuang Liu, Laurens Van Der Maaten, and Kilian Q Weinberger. Densely connected convolutional networks. In *Proceedings of the IEEE conference on computer vision and pattern recognition*, pages 4700–4708, 2017.

Christian Szegedy, Vincent Vanhoucke, Sergey Ioffe, Jon Shlens, and Zbigniew Wojna. Rethinking the inception architecture for computer vision. In *Proceedings of the IEEE conference on computer vision and pattern recognition*, pages 2818–2826, 2016.

Andrew Howard, Mark Sandler, Grace Chu, Liang-Chieh Chen, Bo Chen, Mingxing Tan, Weijun Wang, Yukun Zhu, Ruoming Pang, Vijay Vasudevan, et al. Searching for mobilenetv3. In *Proceedings of the IEEE/CVF International Conference on Computer Vision*, pages 1314–1324, 2019.

Mingxing Tan and Quoc Le. Efficientnet: Rethinking model scaling for convolutional neural networks. In *International Conference on Machine Learning*, pages 6105–6114. PMLR, 2019.

Martin Heusel, Hubert Ramsauer, Thomas Unterthiner, Bernhard Nessler, and Sepp Hochreiter. Gans trained by a two time-scale update rule converge to a local nash equilibrium. *Advances in neural information processing systems*, 30, 2017.

Dan Hendrycks, Mantas Mazeika, and Thomas Dietterich. Deep anomaly detection with outlier exposure. *arXiv preprint arXiv:1812.04606*, 2018.

Benjamin Recht, Rebecca Roelofs, Ludwig Schmidt, and Vaishaal Shankar. Do imagenet classifiers generalize to imagenet? In *International Conference on Machine Learning*, pages 5389–5400. PMLR, 2019.

A Additional Training Details

In this section, we provide training details for all models used to report results in section 4 of the main paper.

A.1 Classifier Training

MNIST models: For experiments on MNIST, we use 4 convolutional architectures: LeNet, AlexNet, VGG-11 and ResNet-18. Each model has been trained on a single 12 GB TITAN Xp GPU for 100 epochs using SGD as the optimizer with a momentum of 0.9. The initial learning rate used was 0.1 and there are learning rate drops by a factor of 10 at training epochs 40 and 60. The training batch size used for MNIST is 256.

CIFAR-10/100 models: All convolutional classifiers: DenseNet-121, ResNet-50/110, VGG-16, are trained using the Pytorch framework with a single 12 GB TITAN Xp GPU. To train models on CIFAR-10/100, we use the SGD optimiser with a momentum of 0.9 and a weight decay of $5e^{-4}$. We train each model for 350 epochs using 0.1 as the learning rate and a learning rate drop by a factor of 10 at training epochs 150 and 250. We use a training batch size of 128 and augment the training set using random crops and random horizontal flips.

For Vision Transformer (ViT) models trained on CIFAR-10/100, we use 4 12 GB TITAN Xp GPUs to train a single model. We train 4 different ViT models: ViT-B-16/32 and ViT-L-16/32, using an image size of 224×224 and other conventional augmentations including random crop and random horizontal flips. All the ViTs are pretrained on ImageNet-21K. We use a SGD with a momentum of 0.9 and a learning rate of $3e^{-2}$ with a cosine learning rate decay. We use 500 warmup steps for each model and train them for a maximum of 10000 steps. We use a training batch size of 256 for the ViT models.

ImageNet models: For ImageNet, we use pretrained Vision Transformers for all evaluation purposes.⁴

Classifier Suite for computing \mathcal{L}_{MI} Note that in order to compute \mathcal{L}_{MI} , we use a single ensemble containing models, each with a different architecture. For MNIST experiments, we use 4 different models: LeNet, AlexNet, VGG-11 and ResNet-18 (one model of each architecture) as the ensemble to compute mutual information over. Similarly, for CIFAR-10/100, we use 6 models with 6 different architectures: DenseNet-121, ResNet-50/110, VGG-16, Wide-ResNet-28-10 and Inception-v3. Finally, for ImageNet, we use a set of pretrained classifiers from the Pytorch `torchvision.models` library. In particular, we get ResNet-18, MobileNet-v3-Large and EfficientNet-B0. Note that the use of ensembles with different architectures is to encourage higher variability in predictions and representations within the ensemble, thereby encouraging higher mutual information for predictions. Ensembles used for the evaluation of generated samples all have the same architecture. All the classifiers used for computing \mathcal{L}_{MI} are trained using the same dataset-specific settings as mentioned above.

A.2 Training Pix-2-Pix GAN

In order to train a Pix-2-Pix GAN, we use $\mathcal{L}_{\text{Shift}}$ defined in eq. (3) as the loss function for the generator of the GAN and there is no change to the loss of the discriminator. However, note that the target image for the Pix-2-Pix discriminator is the same as the input. Thus the loss of the discriminator can be given as:

$$\begin{aligned} \mathcal{L}_{D_{\text{Pix-2-Pix}}} = & \mathbb{E}_{\mathbf{x}} [\log(D(\mathbf{x}, \mathbf{x}))] - \\ & \mathbb{E}_{\mathbf{x}, \mathbf{z}} [\log(1 - D(\mathbf{x}, G(\mathbf{x}, \mathbf{z})))] \end{aligned} \quad (5)$$

For \mathcal{L}_{MI} , in eq. (3), we use the method specified above. We use a single 12 GB TITAN Xp GPU to train the Pix-2-Pix model on CIFAR-10 and 8 such GPUs to train on ImageNet. We use a training batch size of 256 and train the model for 100 epochs using Adam as the optimizer, a learning rate of 0.0002 and beta values 0.5 and 0.999. All other training settings are the same as specified in the original Pix-2-Pix paper Isola et al. [2017].

A.3 Training GAN

For generating Near OoD samples (i.e., Near OoD), we use a DCGAN for MNIST and a BigGAN for CIFAR-10/100 and ImageNet. We use a single 12 GB TITAN Xp GPU to train DCGAN for MNIST and BigGAN for CIFAR-10/100. However, we use 8 such GPUs to train a single BigGAN on ImageNet. The loss function for the discriminator of the GAN undergoes no change and is shown as follows:

$$\mathcal{L}_{D_{\text{GAN}}} = \mathbb{E}_{\mathbf{x}} [\log D(\mathbf{x})] - \mathbb{E}_{\mathbf{z}} [\log(1 - D(G(\mathbf{z})))] \quad (6)$$

⁴See github.com/rwightman/pytorch-image-models for details.

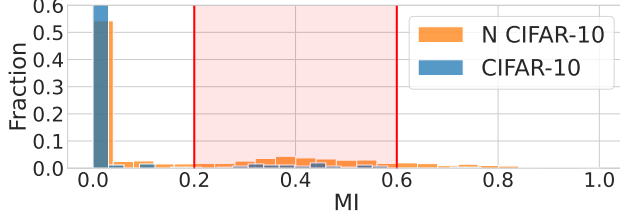


Figure 9: MI of the ensemble for Near OoD (N) CIFAR-10 and real CIFAR-10 samples. We use this to find plausible thresholds of MI.

Model	Test Accuracy	AUROC %			
		F-MNIST (SE)	F-MNIST (SC)	N-MNIST (Ours) (SE)	N-MNIST (Ours) (SC)
LeNet	98.97 \pm 0.02	98.87 \pm 0.05	98.80 \pm 0.05	65.29 \pm 0.12	64.14 \pm 0.11
AlexNet	99.04 \pm 0.03	99.10 \pm 0.05	99.07 \pm 0.05	70.31 \pm 0.15	69.64 \pm 0.13
VGG-11	99.35 \pm 0.02	99.20 \pm 0.04	99.17 \pm 0.03	72.11 \pm 0.13	71.85 \pm 0.13
ResNet-18	99.54 \pm 0.02	99.16 \pm 0.03	99.14 \pm 0.04	73.15 \pm 0.13	72.81 \pm 0.12

Table 4: AUROC % on MNIST using softmax entropy (SE) and softmax confidence (SC) with Fashion(F)-MNIST and Near OoD(N)-MNIST as OoD.

The loss function for the generator is $\mathcal{L}_{\text{Near OoD}}$ as shown in eq. (4). The \mathcal{L}_{MI} in $\mathcal{L}_{\text{Near OoD}}$ is computed as described above. We train all GANs for 100 epochs and all other training details for the GANs are exactly the same as set out in their respective repositories.⁵

A.4 Outlier Exposure

In the outlier exposure experiment, we train a ResNet-50 and a Wide-ResNet-28-10 on CIFAR-100 using the standard training procedure set out in appendix A.1. However, in the loss, following Hendrycks et al. [2018], in addition to the cross-entropy term, we also have an additional regulariser which computes the cross-entropy of the output with a uniform distribution for outlier samples.

B Additional Results

In this section, we present additional results to support the results in the main paper.

MI overlap: In fig. 9, we show the mutual information of the training ensemble on real CIFAR-10 samples along with Near OoD generated samples on CIFAR-10. We choose samples which minimise MI overlap between real and generated samples without having a very high MI as that leads to generated samples losing their perceptual similarity with iD. For CIFAR-10, we choose [0.2, 0.6] as the MI interval for generated samples.

OoD Detection on Near OoD Datasets In table 4, we present test set accuracy and AUROC scores of models trained on MNIST on the MNIST vs Fashion-MNIST and MNIST vs Near OoD MNIST. In table 5, we report the CIFAR-10/100 and ImageNet test set accuracy of all the models we use to evaluate our benchmark. In table 12 and table 14, we report the AUROC scores of 6 convolutional models: DenseNet-121, ResNet-50/110, VGG-16, Wide-ResNet-28-10 and Inception-v3 and 4 Vision Transformer models: ViT-B-16/32, ViT-L-16/32 trained on CIFAR-10 and CIFAR-100 respectively. The uncertainty computation method here uses the softmax entropy, softmax confidence and Mahalanobis distance computed from a single deterministic model. We also compute the AUROC scores for a deep ensemble of size 5, using the 6 convolutional architectures and report the corresponding results in table 7 and table 9 for models trained on CIFAR-10 and CIFAR-100 respectively. For CIFAR-10, we use SVHN, CIFAR-100 and Near OoD CIFAR-10 as OoD sets and for CIFAR-100, we use SVHN, CIFAR-10 and Near OoD CIFAR-100 as OoD sets. The corresponding AUPRC scores for all models trained on CIFAR-10 and CIFAR-100 are shown in table 13 and table 15 for deterministic models and table 8 and table 10 for deep ensembles respectively. In addition, we also show the AUPRC scores as plots for deterministic models, deep ensembles and Vision Transformers in fig. 11. Finally, we report AUPRC scores for Vision Transformer models trained on ImageNet using ImageNet-O and Near OoD ImageNet as OoD datasets in table 6.

Evaluation of Shifted Datasets We present the ECE% of 6 architectures: DenseNet-121, ResNet-50/110, VGG-16, Wide-ResNet-28-10 and Inception-v3, all trained on CIFAR-10 on CIFAR-10-C where we use 15 different corruption

⁵See github.com/ajbrock/BigGAN-PyTorch for details on training BigGAN.

Model	Test/Val Set Accuracy		
	CIFAR-10	CIFAR-100	ImageNet
DenseNet-121	95.66 \pm 0.05	80.08 \pm 0.15	—
ResNet-50	95.34 \pm 0.05	78.26 \pm 0.33	—
ResNet-110	95.50 \pm 0.12	79.50 \pm 0.27	—
VGG-16	93.81 \pm 0.09	74.33 \pm 0.18	—
Wide-ResNet-28-10	96.33 \pm 0.07	80.60 \pm 0.11	—
Inception-v3	95.25 \pm 0.10	78.04 \pm 0.14	—
ViT-B-16	99.12 \pm 0.03	92.73 \pm 0.04	85.02
ViT-B-32	98.73 \pm 0.01	92.14 \pm 0.02	84.72
ViT-L-16	99.18 \pm 0.01	93.73 \pm 0.04	86.55
ViT-L-32	99.02 \pm 0.01	93.29 \pm 0.04	85.47

Table 5: CIFAR-10/100 test and ImageNet val accuracy for CNNs and ViTs used in our evaluation.

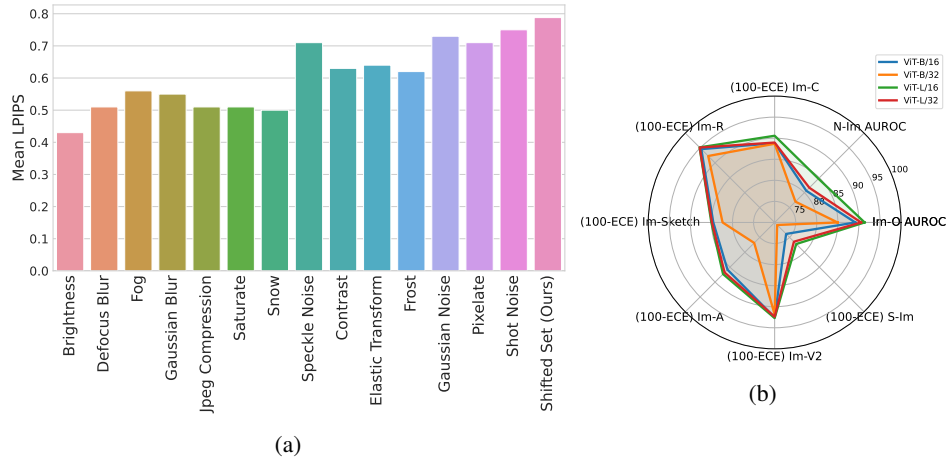


Figure 10: (a) average LPIPS between ImageNet val and corrupted samples, (b) performance of the 4 ViT architectures on all ImageNet benchmarks: ImageNet-C (Im-C), ImageNet-R (Im-R), ImageNet-O (Im-O), ImageNet-A(Im-A), ImageNet-V2(Im-V2), ImageNet-Sketch (Im-Sketch) and our benchmarks Near OoD ImageNet (N-Im) and Shifted ImageNet (S-Im).

types at the highest intensity (i.e., 5) and compare with the ECE% of shifted CIFAR-10. Similarly, we present the ECE% of 4 ViTs: ViT-B-16, ViT-B-32, ViT-L-16 and ViT-L-32, trained on ImageNet, evaluated on ImageNet-C. The results are presented in fig. 12. Clearly, the ECE of shifted CIFAR-10 and shifted ImageNet is significantly higher than all corruption types.

In fig. 10a, we present the LPIPS between images of the ImageNet val set with those corrupted using ImageNet-C corruptions and Shifted ImageNet, where the sample pairs have the same L2 difference in image space. We note that for Shifted ImageNet, the LPIPS is the highest compared to other corruption types. In fig. 10b, we present the radar plot of performance for all ViT models on ImageNet benchmarks. We note that the order of performance remains exactly the same for our benchmarks compared to real-world ImageNet benchmarks.

C Qualitative Examples of Generated Samples

In fig. 13, fig. 14 and fig. 15, we present additional qualitative samples of shifted and near OoD examples respectively for both CIFAR-10, CIFAR-100 and ImageNet. In fig. 13, on the left column, we show real samples from CIFAR-10 and CIFAR-100. On the right column, we show corresponding shifted samples. Similar examples for ImageNet can be found in fig. 14. Finally, in fig. 15, we show examples of near OoD samples for both CIFAR-10, CIFAR-100 and ImageNet.

Model	AUPRC			
	Im-O (SE)	Im-O (SC)	N-Im (Ours) (SE)	N-Im(Ours) (SC)
ViT-B-16	73.23	72.57	67.10	62.08
ViT-B-32	69.39	67.48	55.32	52.24
ViT-L-16	80.46	79.39	70.17	69.58
ViT-L-32	76.15	75.32	68.56	66.93

Table 6: AUPRC of Vision-Transformer models trained on ImageNet using ImageNet-O Hendrycks et al. [2021] (Im-O) and Near OoD ImageNet (N-Im) as OoD datasets and with softmax entropy (SE) and confidence (SC) as uncertainty/confidence.

Model	AUROC		
	SVHN	CIFAR-100	N CIFAR-10
DenseNet-121	97.52	91.42	85.67
ResNet-50	96.24	90.89	84.66
ResNet-110	96.75	91.3	85.55
VGG-16	91.26	89.16	81.07
Wide-ResNet-28-10	96.59	91.78	86.54
Inception-v3	96.12	91.31	87.07

Table 7: AUROC of ensemble models trained on CIFAR-10 using predictive entropy on SVHN, CIFAR-100 and Near OoD CIFAR-10 (N CIFAR-10).

Model	AUPRC		
	SVHN	CIFAR-10	N CIFAR-100
DenseNet-121	98.83	90.72	86.92
ResNet-50	97.87	89.7	85.83
ResNet-110	98.19	90.35	86.7
VGG-16	94.89	87.97	83.93
Wide-ResNet-28-10	98.06	90.94	88.03
Inception-v3	97.79	90.14	88.14

Table 8: AUPRC of ensemble models trained on CIFAR-10 using predictive entropy on SVHN, CIFAR-100 and Near OoD CIFAR-10 (N CIFAR-10).

Model	AUROC		
	SVHN	CIFAR-10	N CIFAR-100
DenseNet-121	88.75	82.92	62.33
ResNet-50	82.66	81.28	57.18
ResNet-110	81.07	82.55	59.7
VGG-16	78.3	78.87	52.42
Wide-ResNet-28-10	83.62	82.65	62.83
Inception-v3	83.89	83.3	64.66

Table 9: AUROC of ensemble models trained on CIFAR-100 using predictive entropy on SVHN, CIFAR-10 and Near OoD CIFAR-100.

Model	AUPRC		
	SVHN	CIFAR-10	N CIFAR-100
DenseNet-121	93.97	78.96	67.82
ResNet-50	90.24	76.78	64.85
ResNet-110	89.08	78.67	66.21
VGG-16	88.27	74.51	62.7
Wide-ResNet-28-10	91.27	78.81	67.94
Inception-v3	89.81	79.14	68.76

Table 10: AUPRC of ensemble models trained on CIFAR-100 using predictive entropy on SVHN, CIFAR-10 and Near OoD CIFAR-100.

Model	CIFAR-10-C			Shifted CIFAR-10 (Ours)
	Avg ECE %	Max ECE %	ECE %	
DenseNet121	13.69 ± 0.17	25.86 ± 0.40	51.55 ± 0.33	
ResNet-50	13.71 ± 0.48	25.76 ± 1.09	50.07 ± 1.24	
ResNet-110	14.40 ± 0.28	28.03 ± 0.55	52.16 ± 0.66	
VGG-16	17.51 ± 0.22	34.45 ± 0.40	56.25 ± 0.41	
Wide-ResNet-28-10	11.92 ± 0.13	22.87 ± 0.21	49.64 ± 0.43	
Inception-v3	13.47 ± 0.37	25.10 ± 0.71	52.84 ± 0.19	

Table 11: ECE % on CIFAR-10-C compared to Shifted CIFAR-10.

Model	AUROC SVHN			AUROC CIFAR-100			AUROC Near OoD CIFAR-10		
	Entropy	Confidence	Mahalanobis	Entropy	Confidence	Mahalanobis	Entropy	Confidence	Mahalanobis
DenseNet-121	93.12 ± 1.13	92.85 ± 1.11	96.22 ± 0.30	87.23 ± 0.21	87.17 ± 0.22	89.71 ± 0.14	78.81 ± 0.36	79.11 ± 0.34	79.75 ± 0.39
ResNet-50	92.39 ± 0.30	92.17 ± 0.30	92.67 ± 1.35	86.92 ± 0.53	86.78 ± 0.50	88.40 ± 0.33	78.92 ± 0.75	79.09 ± 0.72	79.04 ± 0.57
ResNet-110	91.63 ± 1.82	91.41 ± 1.81	91.94 ± 1.56	87.48 ± 0.09	87.35 ± 0.09	87.91 ± 0.2	78.08 ± 0.49	80.20 ± 0.48	78.14 ± 0.50
VGG-16	86.70 ± 1.05	86.78 ± 1.00	90.93 ± 0.81	83.37 ± 0.22	83.30 ± 0.21	85.94 ± 0.35	73.43 ± 0.55	73.61 ± 0.53	75.46 ± 1.12
Wide-ResNet-28-10	90.98 ± 1.14	90.89 ± 1.09	98.72 ± 0.11	88.60 ± 0.06	88.48 ± 0.06	91.15 ± 0.02	80.56 ± 0.47	81.73 ± 0.46	81.78 ± 0.11
Inception-v3	91.94 ± 0.54	91.77 ± 0.53	93.49 ± 0.79	86.54 ± 0.43	86.42 ± 0.42	89.56 ± 0.28	80.27 ± 0.39	80.41 ± 0.38	83.76 ± 0.43
ViT-B-16	99.65 ± 0.01	99.49 ± 0.01	96.67 ± 0.18	98.33 ± 0.03	98.19 ± 0.03	98.87 ± 0.00	87.00 ± 0.04	87.08 ± .04	86.65 ± 0.22
ViT-B-32	99.65 ± 0.01	99.44 ± 0.02	95.35 ± 0.21	98.10 ± 0.03	97.93 ± 0.03	98.67 ± 0.01	85.33 ± 0.12	85.44 ± .12	86.21 ± 0.23
ViT-L-16	99.76 ± 0.02	99.64 ± 0.01	97.66 ± .42	98.70 ± 0.02	98.61 ± 0.01	99.17 ± 0.01	85.93 ± 0.28	86.15 ± 0.27	89.47 ± 0.25
ViT-L-32	99.78 ± 0.01	99.63 ± 0.02	95.63 ± 0.09	98.45 ± .02	98.29 ± .02	98.80 ± .02	85.25 ± 0.2	85.38 ± 0.20	84.83 ± 0.11

Table 12: AUROC of models trained on CIFAR-10 using softmax entropy (Entropy), softmax confidence (Confidence) and Mahalanobis distance on SVHN, CIFAR-100 and Near OoD CIFAR-10. Near OoD samples are far harder to detect given their consistently low AUROC scores.

Model	AUPRC SVHN			AUPRC CIFAR-100			AUPRC Near OoD CIFAR-10		
	Entropy	Confidence	Mahalanobis	Entropy	Confidence	Mahalanobis	Entropy	Confidence	Mahalanobis
DenseNet-121	96.78 \pm 0.38	82.89 \pm 5.11	94.4 \pm 0.41	86.84 \pm 0.11	84.7 \pm 0.66	89.75 \pm 0.15	80.38 \pm 0.14	63.6 \pm 0.52	68.72 \pm 0.75
ResNet-50	95.88 \pm 0.13	86.19 \pm 1.44	88.41 \pm 2.29	85.85 \pm 0.39	85.39 \pm 0.92	88.45 \pm 0.42	80.97 \pm 0.33	65.81 \pm 1.92	68.86 \pm 1.09
ResNet-110	95.58 \pm 0.95	85.35 \pm 3.25	86.25 \pm 2.29	86.29 \pm 0.14	86.27 \pm 0.23	87.54 \pm 0.29	80.8 \pm 0.28	67.73 \pm 1.26	64.41 \pm 1.2
Wide-ResNet-28-10	95.58 \pm 0.59	77.81 \pm 2.88	97.6 \pm 0.15	88.15 \pm 0.08	85.83 \pm 0.16	91.55 \pm 0.04	80.9 \pm 0.22	66.03 \pm 0.87	72.06 \pm 0.2
Inception-v3	95.7 \pm 0.31	83.32 \pm 1.8	90.91 \pm 0.86	85.86 \pm 0.41	83.14 \pm 0.67	90.13 \pm 0.28	81.47 \pm 0.22	63.45 \pm 0.66	78.11 \pm 0.34
ViT-B-16	99.86 \pm 0.0	99.08 \pm 0.02	93.2 \pm 0.37	98.41 \pm 0.03	98.18 \pm 0.03	98.77 \pm 0.01	92.54 \pm 0.03	76.39 \pm 0.19	76.72 \pm 0.43
ViT-B-32	99.86 \pm 0.01	99.0 \pm 0.04	90.64 \pm 0.42	98.19 \pm 0.03	97.88 \pm 0.02	98.57 \pm 0.01	91.53 \pm 0.08	73.21 \pm 0.15	76.56 \pm 0.6
ViT-L-16	99.9 \pm 0.01	99.36 \pm 0.04	95.42 \pm 0.85	98.8 \pm 0.01	98.49 \pm 0.02	99.02 \pm 0.01	92.68 \pm 0.12	70.26 \pm 0.77	81.19 \pm 0.29
ViT-L-32	99.91 \pm 0.0	99.33 \pm 0.02	90.36 \pm 0.18	98.55 \pm 0.02	98.25 \pm 0.04	98.6 \pm 0.03	92.02 \pm 0.08	69.81 \pm 0.59	73.29 \pm 0.14

Table 13: AUPRC of models trained on CIFAR-10 using softmax entropy (Entropy), softmax confidence (Confidence) and Mahalanobis distance on SVHN, CIFAR-100 and Near OoD CIFAR-10. Near OoD samples are far harder to detect given their consistently low AUPRC scores.

Model	AUROC SVHN			AUROC CIFAR-100			AUROC Near OoD CIFAR-100		
	Entropy	Confidence	Mahalanobis	Entropy	Confidence	Mahalanobis	Entropy	Confidence	Mahalanobis
DenseNet-121	84.52 \pm 1.55	83.13 \pm 1.44	89.49 \pm 0.55	79.73 \pm 0.25	79.12 \pm 0.24	77.26 \pm 0.47	60.32 \pm 0.27	60.5 \pm 0.26	64.16 \pm 0.28
ResNet-50	79.77 \pm 0.69	78.82 \pm 0.71	86.41 \pm 0.11	78.82 \pm 0.08	78.26 \pm 0.09	82.68 \pm 0.18	56.58 \pm 0.26	56.67 \pm 0.26	58.48 \pm 0.67
ResNet-110	77.84 \pm 1.56	77.26 \pm 1.4	86.62 \pm 0.23	79.92 \pm 0.17	79.3 \pm 0.15	82.9 \pm 0.23	58.6 \pm 0.56	58.58 \pm 0.46	59.73 \pm 0.59
VGG-16	76.33 \pm 1.12	75.38 \pm 0.97	78.01 \pm 1.24	74.02 \pm 0.14	73.62 \pm 0.13	74.99 \pm 0.13	51.06 \pm 0.14	51.53 \pm 0.15	56.41 \pm 0.42
Wide-ResNet-28-10	81.85 \pm 0.79	80.71 \pm 0.7	84.18 \pm 1.01	80.82 \pm 0.11	80.41 \pm 0.12	73.42 \pm 0.14	62.19 \pm 0.17	62.05 \pm 0.14	62.38 \pm 0.1
Inception-v3	81.6 \pm 1.64	80.95 \pm 1.46	81.8 \pm 0.57	81.24 \pm 0.18	80.89 \pm 0.18	79.87 \pm 0.22	63.96 \pm 0.85	63.39 \pm 0.78	60.53 \pm 0.97
ViT-B-16	93.31 \pm 0.21	91.92 \pm 0.19	95.91 \pm 0.03	93.29 \pm 0.04	92.35 \pm 0.05	93.95 \pm 0.03	79.47 \pm 0.06	79.04 \pm 0.06	82.91 \pm 0.07
ViT-B-32	92.98 \pm 0.13	91.56 \pm 0.11	93.78 \pm 0.21	91.97 \pm 0.2	90.94 \pm 0.21	92.22 \pm 0.19	75.36 \pm 0.16	75.05 \pm 0.15	78.97 \pm 0.24
ViT-L-16	95.11 \pm 0.16	94.29 \pm 0.15	97.6 \pm 0.04	94.62 \pm 0.08	94.04 \pm 0.09	95.31 \pm 0.09	80.36 \pm 0.08	80.23 \pm 0.1	84.72 \pm 0.21
ViT-L-32	94.01 \pm 0.07	92.62 \pm 0.06	96.01 \pm 0.12	94.09 \pm 0.07	93.28 \pm 0.06	94.15 \pm 0.06	76.87 \pm 0.12	76.64 \pm 0.12	81.29 \pm 0.14

Table 14: AUROC of models trained on CIFAR-100 using softmax entropy (Entropy), softmax confidence (Confidence) and Mahalanobis distance on SVHN, CIFAR-10 and Near OoD CIFAR-100. Near OoD samples are far harder to detect given their consistently low AUROC scores.

Model	AUPRC SVHN			AUPRC CIFAR-100			AUPRC Near OoD CIFAR-100		
	Entropy	Confidence	Mahalanobis	Entropy	Confidence	Mahalanobis	Entropy	Confidence	Mahalanobis
DenseNet-121	91.84 \pm 0.93	72.78 \pm 2.29	82.85 \pm 0.73	75.89 \pm 0.3	80.67 \pm 0.38	80.31 \pm 0.26	69.17 \pm 0.13	50.01 \pm 0.6	55.53 \pm 0.3
ResNet-50	88.69 \pm 0.28	67.45 \pm 1.23	81.58 \pm 0.51	74.4 \pm 0.14	80.26 \pm 0.18	85.78 \pm 0.45	66.07 \pm 0.15	50.27 \pm 0.6	50.33 \pm 0.91
ResNet-110	87.29 \pm 1.01	62.34 \pm 2.97	81.9 \pm 0.78	75.94 \pm 0.17	81.25 \pm 0.23	86.1 \pm 0.55	67.37 \pm 0.35	48.07 \pm 1.02	51.08 \pm 0.99
VGG-16	87.04 \pm 0.78	60.21 \pm 1.61	66.7 \pm 1.54	70.35 \pm 0.18	73.07 \pm 0.23	77.02 \pm 0.25	64.3 \pm 0.07	50.72 \pm 0.17	50.32 \pm 0.39
Wide-ResNet-28-10	90.27 \pm 0.55	69.98 \pm 1.23	72.42 \pm 0.92	76.76 \pm 0.17	82.41 \pm 0.11	76.36 \pm 0.15	68.98 \pm 0.09	55.56 \pm 0.19	54.03 \pm 0.13
Inception-v3	88.54 \pm 1.19	72.75 \pm 2.25	66.81 \pm 2.55	76.89 \pm 0.3	82.99 \pm 0.1	79.31 \pm 0.35	69.98 \pm 0.34	59.6 \pm 1.21	50.77 \pm 1.07
ViT-B-16	97.24 \pm 0.08	83.16 \pm 0.85	93.22 \pm 0.06	93.73 \pm 0.03	92.68 \pm 0.06	94.4 \pm 0.02	87.15 \pm 0.02	66.33 \pm 0.15	74.84 \pm 0.18
ViT-B-32	97.1 \pm 0.06	82.0 \pm 0.69	90.46 \pm 0.28	92.79 \pm 0.18	90.93 \pm 0.21	92.66 \pm 0.25	84.23 \pm 0.15	60.24 \pm 0.12	69.31 \pm 0.4
ViT-L-16	98.08 \pm 0.06	84.33 \pm 0.89	94.92 \pm 0.09	95.11 \pm 0.06	93.89 \pm 0.12	95.43 \pm 0.08	88.25 \pm 0.05	63.66 \pm 0.21	76.63 \pm 0.33
ViT-L-32	97.58 \pm 0.01	83.2 \pm 0.41	93.4 \pm 0.23	94.65 \pm 0.06	93.2 \pm 0.08	94.66 \pm 0.07	85.8 \pm 0.06	58.91 \pm 0.24	72.46 \pm 0.21

Table 15: AUPRC of models trained on CIFAR-100 using softmax entropy (Entropy), softmax confidence (Confidence) and Mahalanobis distance on SVHN, CIFAR-10 and Near OoD CIFAR-100. Near OoD samples are far harder to detect given their consistently low AUPRC scores.

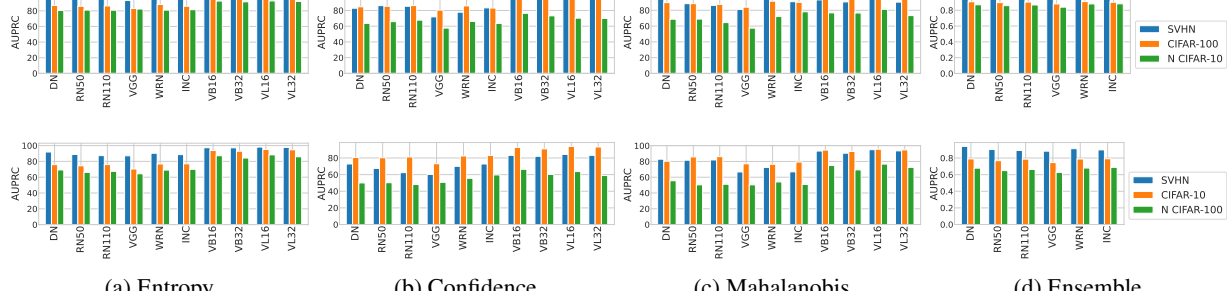


Figure 11: AUPRC % for different models, DenseNet-121 (DN), ResNet-50 (RN50), ResNet-110 (RN110), VGG-16, Wide-ResNet-28-10 (WRN) and Inception-v3 (INC), ViT-B-16/32 (VB16/32) and ViT-L-16/32 (VL16/32) trained on CIFAR-10 and CIFAR-100 using SVHN, CIFAR-10/100 and Near OoD (N) CIFAR-10/100 as OoD datasets and softmax entropy, confidence, Mahalanobis distance and deep ensemble baselines.

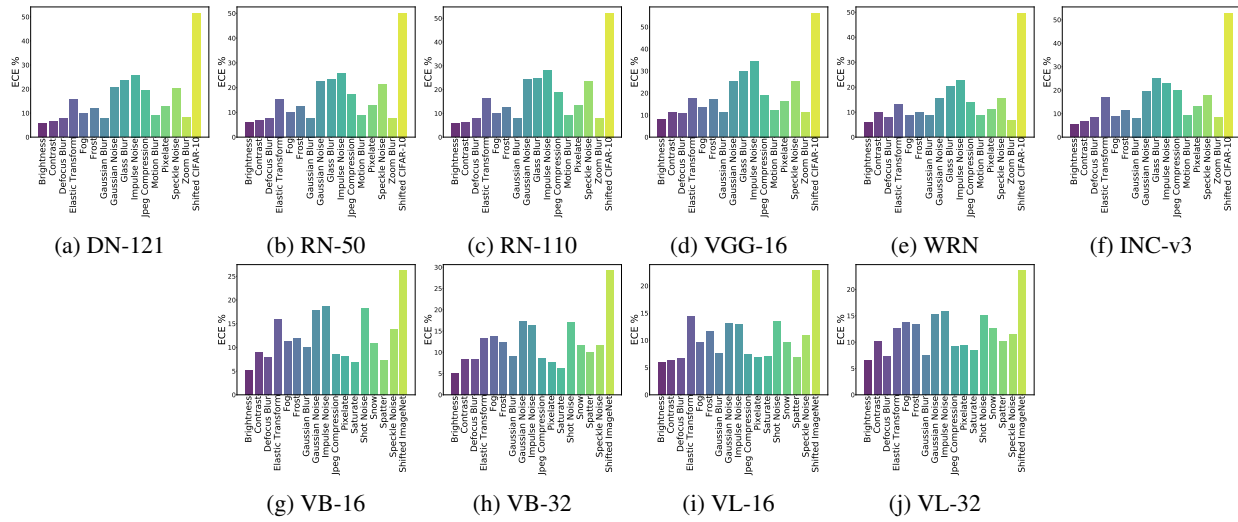
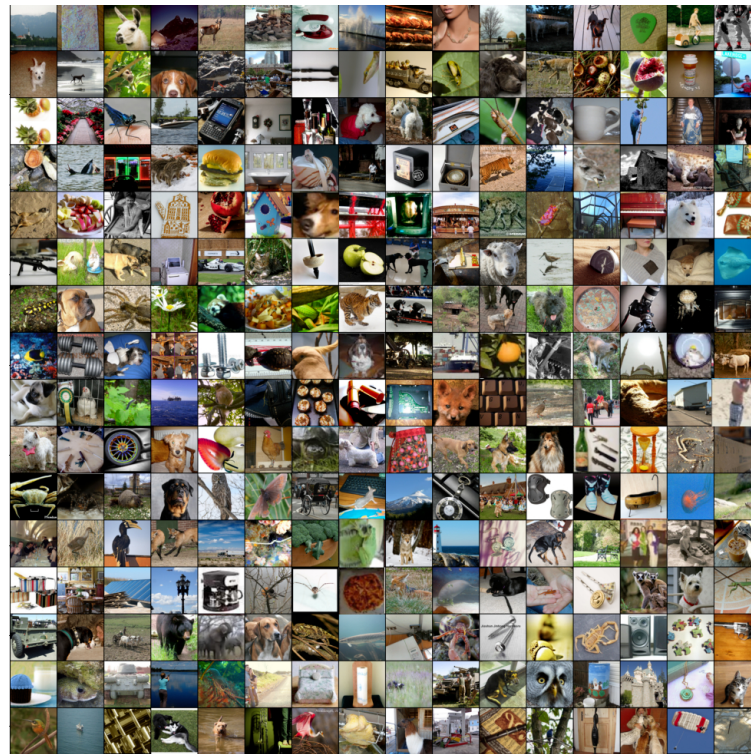


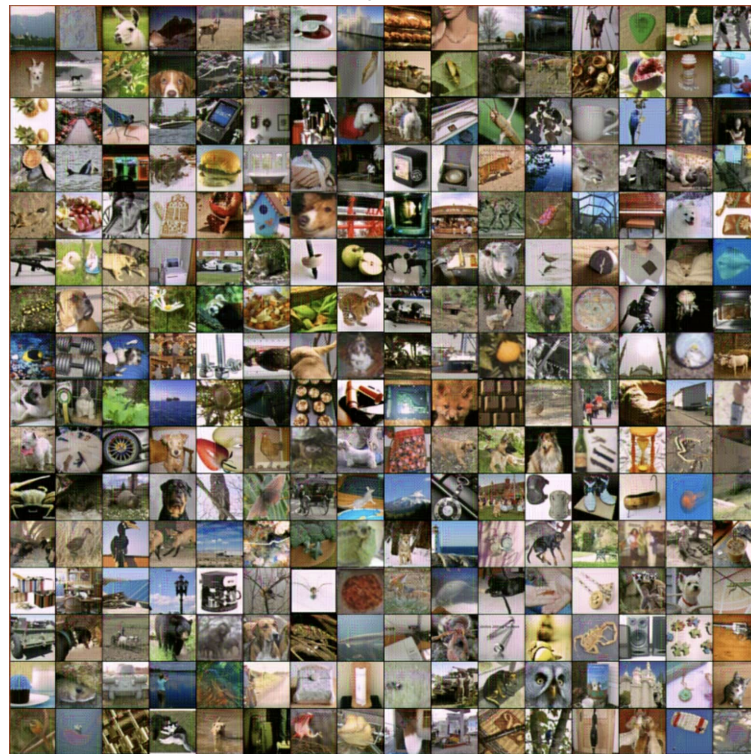
Figure 12: ECE% of models on CIFAR-10-C (top row) and ImageNet-C (bottom row) for different corruption types.



Figure 13: Additional qualitative samples for CIFAR-10 and CIFAR-100 datasets. Left column shows real samples, and the right column shows corresponding shifted/transformed samples.



(a) ImageNet Real



(b) ImageNet Shifted

Figure 14: Additional qualitative samples for ImageNet datasets. Top shows real samples, and bottom shows corresponding shifted/transformed samples.



Figure 15: Additional qualitative samples for CIFAR-10, CIFAR-100 and ImageNet datasets. Samples show Near OoD images.